Magnetic and electronic properties of $Ca_{1-x}Na_xCr_2O_4$: Double-exchange interactions and ligand holes

Hiroya Sakurai*

National Institute for Materials Science, 1-1 Namiki, Tsukuba 305-0044, Japan

(Received 13 September 2013; revised manuscript received 17 December 2013; published 27 January 2014)

β-$CaCr_2O_4$ has a cycloidal magnetic structure and isostructural $NaCr_2O_4$ shows unconventional colossal magnetoresistance below a canted antiferromagnetic (AFM) ordering temperature of $T_N = 125$ K. In this paper, magnetic and electronic properties of the solid-solution system $Ca_{1-x}Na_xCr_2O_4$, are investigated. The T_N value decreases with decreasing x from $x = 1$ to $\frac{2}{3}$. A spin-glass behavior appears for $0.1 \leqslant x \leqslant 0.6$. Interestingly, the spin-glass character is detected even for $\frac{2}{3} \leqslant x \leqslant 0.95$ coexisting with the AFM ordering. Curie constant increases and Weiss temperature decreases with decreasing x. Curie constant is significantly suppressed from theoretical value, suggesting large quantum fluctuations and strong hybridization between Cr and O ions for higher-x values. Substitution of Ca for Na introduces the ligand holes. The decrease in Weiss temperature points out that a single ligand hole mediates ferromagnetic interaction of approximately 400 K by the double-exchange mechanism. Saturation magnetization and magnetic susceptibility at 2 K show unusual x dependencies, which suggests that not only the canting angle but also the periodicity of magnetic ordering depend on x. Electrical resistivity for $0.2 \leqslant x \leqslant 0.95$ follows the variable-range hopping mechanism, suggesting Anderson localization at the x range.

DOI: 10.1103/PhysRevB.89.024416 PACS number(s): 75.30.Et, 75.30.Cr, 75.47.Lx

I. INTRODUCTION

In oxides, transition-metal (TM) ions with extremely high formal valence, such as Fe^{4+}, Ni^{3+}, and Cu^{3+}, create holes on the ligand oxygens because of their deep energy level of $3d$ orbitals relative to the oxygen $2p$ level. This means that these oxides have negative charge-transfer energy E_{CT}. Many TM oxides with negative E_{CT} show interesting properties such as metal-insulator transitions due to charge disproportionation in AFe(IV)O_3 (A = Sr and Ca) and RNi(III)O_3 (R: lanthanoid element and Y) [1–4]. High-T_C superconductivity also may be regarded as the property of the TM oxides with negative E_{CT} because it occurs when holes are introduced into certain copper oxides with Cu^{2+} ions.

In some cases, a ferromagnetic (FM) state is found in the TM oxides with negative E_{CT}, such as CrO_2 [5] and $K_2Cr_8O_{16}$ [6–9]. The FM interactions in the latter two compounds are mediated by ligand holes, and so can be regarded as double-exchange (DE) interactions [5,8]. This type of the DE interaction is characteristic in that the ligand holes carry the interactions: In the case of conventional DE interactions in Mn perovskites, e_g electrons on neighboring Mn ions cause the FM interactions through the Hund coupling [10–12]. On the other hand, a ligand hole is antiferromagnetically coupled with the d electrons on a TM ion through a strong hybridization between the TM ion and the ligand oxygen, as in the case of Zhang-Rice singlet formation in the high-T_C cuprates [13]. If the oxygen ion is shared by two TM ions, effective FM interactions occur between two spins of the d electrons through the antiferromagnetic (AFM) interactions between the ligand hole and the d electrons. Obviously, this mechanism will work even when the hole is localized on an oxygen ion. Although a similar mechanism of the DE interaction has recently been theoretically proposed for the Peierls insulator state [14], few studies have addressed the DE interactions mediated by ligand holes.

β-$CaCr_2O_4$ and $NaCr_2O_4$ crystallize in calcium-ferrite-type structure, which is composed of double rutile chains as shown in Fig. 1. β-$CaCr_2O_4$ is electrically insulating and has cycloidal magnetic structure below $T_N = 21$ K due to spin frustrations in the chains [15]. On the other hand, $NaCr_2O_4$ shows a canted AFM transition at $T_N = 125$ K. Under zero magnetic field, its electrical resistivity obeys Arrhenius-type temperature dependence with energy gap of $\Delta = 543$ or 1334 K below or above T_N, respectively. Under a magnetic field of 9 T, it does not show a divergent resistivity behavior at 0 K due to the colossal magnetoresistance (CMR) effect developing with decreasing temperature [16,17]. $NaCr_2O_4$ has negative E_{CT} because it has high-valence Cr^{4+} ions as in the case of CrO_2 and $K_2Cr_8O_{16}$. In fact, the holes on oxygen ions have been confirmed by x-ray absorption spectroscopy of O-K edge [18] and have also been observed in the measurements of the Seebeck coefficient [19]. Electronic band-structure calculation indicates that the holes are localized at O(3) sites [20]. Thus, the β-$CaCr_2O_4$–$NaCr_2O_4$ solid solution gives a chance to study the effect of the ligand hole density on the magnetism as the Cr valence increases from +3 for β-$CaCr_2O_4$ to +3.5 for $NaCr_2O_4$. In addition, the transport properties of the solid-solution system are of interest because of the CMR effect reported for the $NaCr_2O_4$ end member.

II. EXPERIMENT

Powder samples of $Ca_{1-x}Na_xCr_2O_4$ ($0 < x < 1$) were synthesized at 1300 °C under high pressure of 6 GPa. A stoichiometric mixture of CaO, Na_2O_2, and Cr_2O_3 was weighed, mixed and sealed in a gold capsule in a glove box filled with Ar gas. The sample was pressed in a belt-type press and then heated for one hour. The temperature was quenched to ambient after the synthesis and then the pressure was gradually

*sakurai.hiroya@nims.go.jp

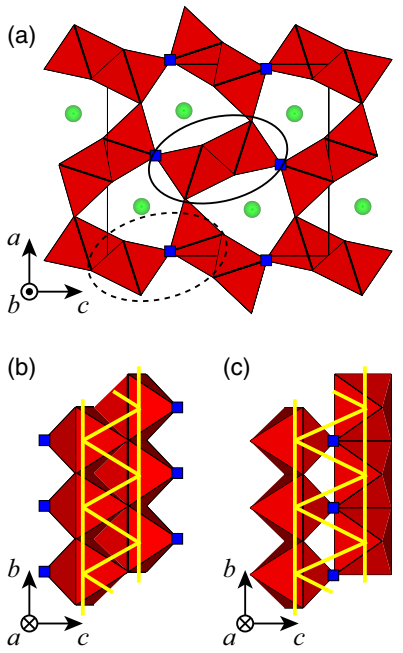

FIG. 1. (Color online) Crystal structure of $NaCr_2O_4$. The octahedra (red), circles (green), and blue squares represent CrO_6 octahedra, Na sites, and O(3) sites, respectively. Panels (b) and (c) show the octahedra in the solid and broken ovals in panel (a), respectively. The yellow lines connect Cr sites.

released. Some samples were made using $NaCrO_2$ as Na source instead of Na_2O_2. Their magnetic properties perfectly agree with similar samples made from Na_2O_2. $NaCr_2O_4$ was made from $NaCrO_2$, Cr_2O_3, and CrO_3 at 1300 °C under 7 GPa [16]. β-$CaCr_2O_4$ was made by two methods. One is the high-pressure synthesis from CaO and Cr_2O_3, and the other is conventional solid-state reaction under ambient pressure; the stoichiometric mixture of $CaCO_3$ and Cr_2O_3 was fired twice in flowing Ar gas at 1300 °C for ∼12 h with an intermediate regrinding. There was no difference in magnetic properties between the two β-$CaCr_2O_4$ samples. All the samples except $NaCr_2O_4$ were proven to be single phase by powder x-ray diffraction measurement. $NaCr_2O_4$ sample contained a small amount of impurities. The stoichiometry of the target compound was not affected by impurities, as discussed in Ref. [16].

Magnetic data were collected on MPMS-XL (Quantum Design). Electrical resistivity and specific heat were measured using PPMS (Quantum Design). Magnetization curves were measured from 7 to −0.1 T. Temperature dependence of magnetization was measured under 0.001 and 1 T for $T \leqslant 320$ K and under 5 T for $T \geqslant 300$ K. Magnetization data under 0.001 T were collected for each sample under zero-field-cooling (ZFC) and field-cooling (FC) conditions. The magnet of MPMS-XL was quenched by heating to achieve zero magnetic field before the sample was loaded into the machine. The resistivity measurement was performed by the conventional four-probe method using a press-contact assembly, PC-RES-P, produced by Wimbush Science & Technology. The pellets used were very dense because they were sintered under the high pressure: For example, the bulk density of

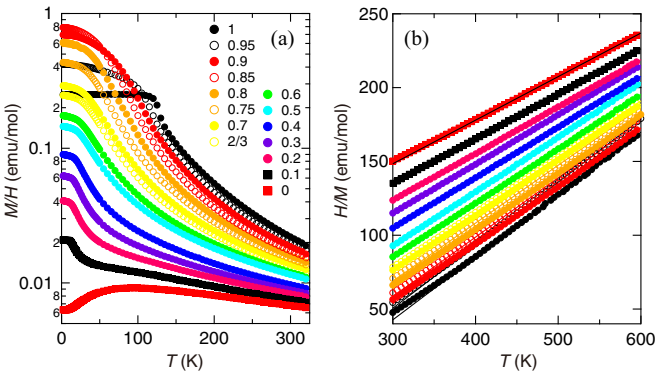

FIG. 2. (Color online) Temperature dependence of magnetization of $Ca_{1-x}Na_xCr_2O_4$ measured under 1 T (a) and 5 T (b). Log scale is used for the vertical axis in panel (a). The lines in panel (b) represent the results of Curie-Weiss fitting. For monochromatic printouts, the M/H value at 300 K decreases with decreasing x.

4.44 g/cm^3 for β-$CaCr_2O_4$, and 4.33 g/cm^3 for $NaCr_2O_4$ was achieved, which correspond to 92.2% and 93.5% of the ideal values, respectively. In this paper, T, H, M, M_S, χ, ρ, and C_P represent temperature, magnetic field, magnetization, spontaneous magnetization, magnetic susceptibility, electrical resistivity, and specific heat, respectively. Magnetic susceptibility is defined as the slope of magnetization curve.

III. RESULTS AND DISCUSSION

Temperature dependence of M/H measured under 1-T FC condition is shown in Fig. 2. The M/H-T curves of all the samples obey Curie-Weiss law of $\chi = C/(T - \Theta)$ at a high temperature. Curie constant C and Weiss temperature Θ estimated from the H/M data between 450 and 600 K by a linear function are summarized in Fig. 3. Curie constant is significantly smaller than the theoretical value calculated assuming $S = \frac{3}{2}$ and 1 for Cr^{3+} and Cr^{4+}, respectively, and g value of 2. The g values were calculated from the C values to be $g = 1.9$ and 1.8 for $x = 0$ and 1, respectively, although g values of Cr^{3+} ions are typically between 1.97

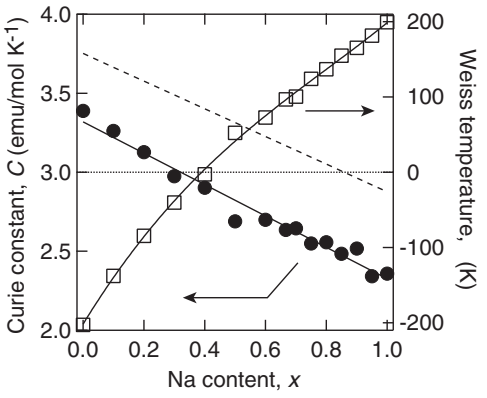

FIG. 3. Curie constant C (closed circles) and Weiss temperature Θ (open squares) as functions of Na content x. The solid lines are guides for the eye, and the broken line shows the theoretical value of C.

and 2.00 [21–25]. The major origins of reduction of g value are, in general, quantum fluctuations and covalency between magnetic and ligand ions. The reduction of the g value from 2 to 1.9 is probably caused by the quantum fluctuations because β-$CaCr_2O_4$ shows cycloidal magnetic structure due to spin frustrations [15] in which some of the magnetic moments diminish by quantum fluctuations. On the other hand, the additional reduction from $g = 1.9$ to 1.8 at $x = 1$ would be caused by the covalency because higher covalency is expected as more ligand holes are introduced through the hybridization between Cr and O ions. Indeed, the deviation of the observed Curie constant from the theoretical one becomes larger with increasing x values, namely, with increasing the number of ligand holes.

Previously, Curie constant of β-$CaCr_2O_4$ was estimated to be 3.89 emu K/mol from the data between 350 and 400 K [15]. The value is largely different from that estimated in this paper and is slightly larger than the theoretical value of 3.75 emu K/mol, which means that $g > 2$. The previous value was probably overestimated. The g value should be smaller than 2 because Cr $3d$ orbitals are less than half-filled. Indeed, to our best knowledge, no Cr oxide has Cr ions with g value more than 2 in a paramagnetic state [21–25]. The temperatures for the Curie-Weiss fit in Ref. [15] were too low as shown in Fig. 2(b); at the temperatures, the magnetic susceptibility deviates from Curie-Weiss law due to short-range ordering of Cr spins.

Weiss temperature almost linearly increases with increasing x from -202 to $+199$ K, suggesting that a hole mediates FM interaction of approximately $+400$ K. It is larger than the double-exchange interaction of 10.6 meV ($=123$ K) in metallic state of $K_2Cr_8O_{16}$ [8], but is still comparable. The FM interaction of $+400$ K is comparable also with FM interaction induced in $La_{2-x}Sr_xCoO_4$ by increasing the x value [26]. Weiss temperature of the Co compound almost linearly increases from -200 K for $x = 0.4$ to $+200$ K for $x = 1.4$, although it is not clear whether the change in Weiss temperature is simply caused by the ligand holes because the spin states also change depending on the x value [27]. On the other hand, Weiss temperature of $Ca_{1-x}La_xMnO_3$ does not increase linearly [28]; it increases very rapidly with the slope of $+17\,800$ K at $x \sim 0$ (-565 K for $x = 0$ and -209 K for $x = 0.02$) but the slope decreases at higher x. The Weiss temperature increases only up to 73.1 K at $x = 0.1$ and appears to be almost saturated there. The difference in both the magnitude and x dependence of Θ may be attributed to different mechanisms of the double-exchange interactions; the FM interaction in $NaCr_2O_4$ is caused by the ligand holes, while that in the Mn oxide by the e_g electrons.

According to the band calculation [20], holes are located on an O(3) site, which bridges the double rutile chains. So, the FM interaction occurs between the double rutile chains. On the other hand, intra-double-chain interactions are most likely comparable to those in β-$CaCr_2O_4$, which has Weiss temperature of -202 K. The intra-double-chain interactions in $NaCr_2O_4$ are caused by superexchange interactions between Cr spins, and the Cr spins are caused mostly by $3d^3$ electrons. Therefore, $NaCr_2O_4$ has almost the same intra-double-chain interactions as β-$CaCr_2O_4$. Thus, it is suggested that the magnetism of $NaCr_2O_4$ is, at least, quasi-two-dimensional with the Cr_2O_4 slabs along the bc plane, whereas that of β-$CaCr_2O_4$ is quasi-one-dimensional showing cycloidal magnetic structure [15].

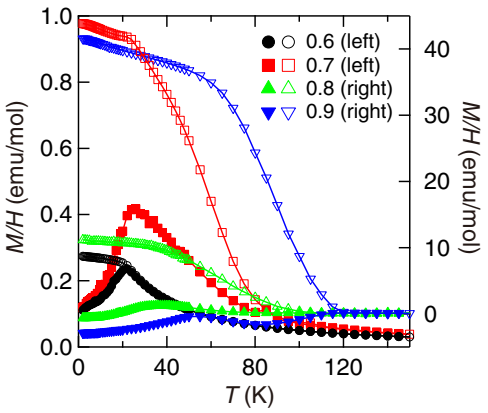

FIG. 4. (Color online) Temperature dependence of magnetization of $Ca_{1-x}Na_xCr_2O_4$ measured under 0.001 T. The left axis is the data for $x = 0.6$ (black circles) and 0.7 (red squares), while the right one for $x = 0.8$ (green upward triangles) and 0.9 (blue downward triangles). The closed and open markers are ZFC and FC data, respectively, and the lines are guides for the eye.

The AFM transition of $NaCr_2O_4$ was clearly detected by the difference between ZFC and FC magnetization because it is accompanied by the appearance of spontaneous magnetization due to the canting of spins. The AFM transition temperature T_N was determined as the temperature where ZFC and FC data separate from each other; the T_N value agrees with the temperature of the peak in specific-heat data [16,17]. Magnetization under FC condition increases steeply below T_N because of the spontaneous magnetization. Both the ZFC and FC separation and a steep increase in FC magnetization were clearly seen also for $Ca_{1-x}Na_xCr_2O_4$ ($\frac{2}{3} \leqslant x \leqslant 0.95$) as shown in Fig. 4. The separation is most likely due to AFM transition because a typical spin-glass transition does not show such a large and steep enhancement of FC magnetization. Preliminary neutron diffraction measurement for $x = 0.85$ has detected magnetic Bragg peaks at 2 K. Therefore, the temperature at the ZFC-FC separation is regarded as T_N here. The compositional dependence of T_N is shown in Fig. 5. T_N decreases with decreasing x down to $x = 0.75$ according to $T_N = 25 + 100x$. The extrapolated T_N value at $x = 0$ is very close to the T_N of β-$CaCr_2O_4$, which was estimated from specific heat [15]. Linear decrease in T_N has been observed also in isostructural $Ca_{1-x}Na_xV_2O_4$ [29].

Below $x = 0.6$, typical spin-glass behavior was observed as shown in Fig. 4. Spin-glass transition temperature T_{SG} is also plotted in Fig. 5. The V oxide also has a spin-glass-like phase next to the AFM phase [30,31]. Interestingly, in case of the Cr oxide, the glassy behavior persists even for $\frac{2}{3} \leqslant x \leqslant 0.95$. There is a peak in the temperature dependence of magnetization under the ZFC condition (see data with $x = 0.7$, 0.8, and 0.9 in Fig. 4). The peak is different from the one which is caused by dynamics of magnetic domains as is typically seen just below the FM transition temperature in many ferromagnets because there is a large difference between magnetizations under ZFC and FC conditions above the peak temperature. In addition, the x dependence of the peak temperature appears

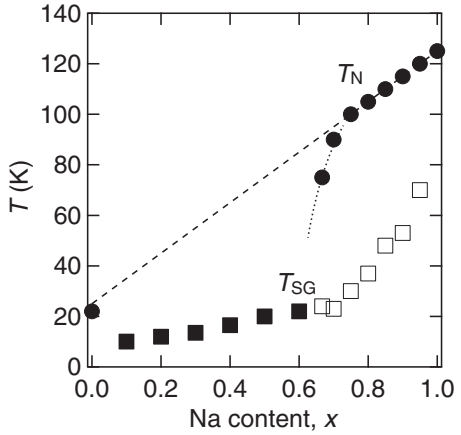

FIG. 5. AFM transition temperature T_N (circles) and spin-glass transition temperature T_{SG} (squares) as functions of Na content x. The open squares show the temperature where ZFC magnetization under 0.001 T has a peak. The broken line is $T_N = 25 + 100x$, and the dotted line is a guide for the eye.

to be continuous from the x-T_{SG} curve below $x = 0.6$, as seen in Fig. 5. The T_{SG} for $\frac{2}{3} \leqslant x \leqslant 0.95$ was determined by the peak temperature of ZFC magnetization under 0.001 T. The coexistence of the glassy behavior with the canted AFM ordering is not due to the compositional phase separation because the T_N and T_{SG} values clearly depend on the x value. The spin-glass behavior may be caused by local inhomogeneity of magnetic interactions. The ligand holes, which carry the FM interactions, are trapped by random potential due to distribution of Na and Ca ions, as suggested by variable-range hopping of electrical resistivity for $0.2 \leqslant x \leqslant 0.95$ shown in the following. $NaCr_2O_4$ does not show the glassy behavior and its temperature dependence of the resistivity follows Arrhenius-type behavior [16].

Magnetization curves of selected samples are shown in Fig. 6. Spin-flop transitions are seen at $H_C = 3.5$ and 2.5 T for $x = 1$ and 0.95, respectively, while no clear transition is observed for $x \leqslant 0.9$. Only 5% difference in the Cr valence

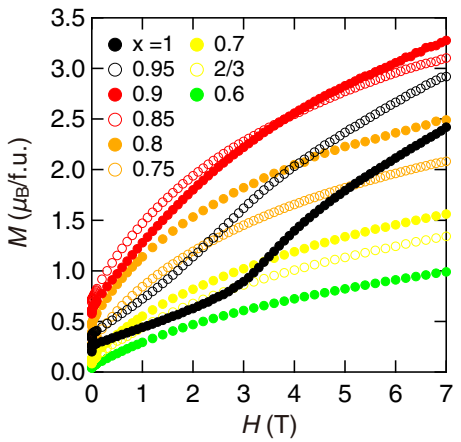

FIG. 6. (Color online) Magnetization curve of $Ca_{1-x}Na_xCr_2O_4$ at 2 K. For monochromatic printouts, the M value at 7 T decreases in the order of $x = 0.9$, 0.85, 0.95, 0.8, 1, 0.75, 0.7, $\frac{2}{3}$, and 0.6.

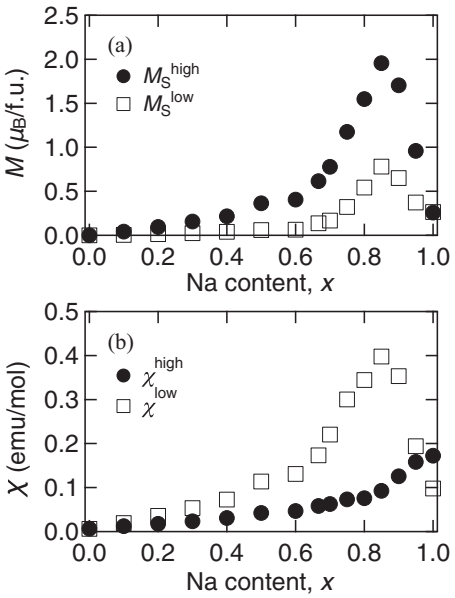

FIG. 7. Spontaneous magnetization (a) and magnetic susceptibility (b) of $Ca_{1-x}Na_xCr_2O_4$ at 2 K. The closed circles and open squares represent the data estimated from the magnetization curves between 0.1 and 1 T and between 6 and 7 T, respectively.

eliminates the transition, which points out that the spin-flop transition is relevant to the spin frustrations [17] and not to the magnetic anisotropy of crystallographic origin. This is because magnetic ordering with spin frustrations is generally very sensitive to the randomness of the interactions, whereas the anisotropy of crystallographic origin is robust. Considering the x-H magnetic phase diagram at 2 K, the AFM phase for $\frac{2}{3} \leqslant x \leqslant 0.9$ corresponds to the AFM phase for $x = 1$ above H_C (phase AF II in Ref. [17]). Also, for $Ca_{1-x}Na_xV_2O_4$, the AFM phase for a lower x value at zero field corresponds to the AFM phase for $x = 1$ at a higher field (phase AF2 in Ref. [29]). These similarities between the V and Cr oxides imply common physical background for the magnetic states. Spin frustrations are the possible background because they are expected for both compounds [17,32].

Spontaneous magnetization at 2 K was estimated from the magnetization curve between 0.1 and 1 T, and between 6 and 7 T. The values for the lower and higher fields are distinguished by the indices "low" and "high," respectively. As shown in Fig. 7, M_S^{low}, M_S^{high}, and χ^{low} reach maxima at $x = 0.85$, although T_N, C, and Θ change monotonically as shown above. The lattice constants also show monotonic dependence on x [16]. If the FM interactions mediated by holes cause only the canting of magnetic moments on Cr ions, the maximum of M_S would occur when the FM interactions are at maximum, namely, at $x = 1$. Obviously, this is not the case, and so it is expected that the periodicity of magnetic structure also depends on x. As supported by preliminary neutron diffraction and muon spin rotation measurements [33], $NaCr_2O_4$ has a commensurate magnetic structure, whereas β-$CaCr_2O_4$ has an incommensurate one [15].

Magnetic susceptibility for $x = 1$, 0.95, and 0.9 is shown together with M/H data in Fig. 8. The magnetic susceptibility for $x = 1$ shows a clear peak at T_N, which is typical of the

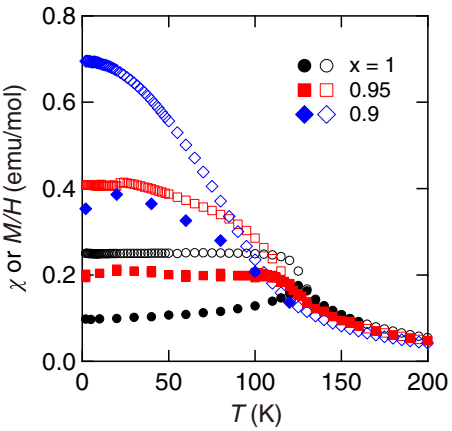

FIG. 8. (Color online) Magnetic susceptibility (closed markers) and M/H under $H = 1$ T (open markers) of of $Ca_{1-x}Na_xCr_2O_4$ ($x = 0.9$, 0.95, and 1). The magnetic susceptibility was estimated from magnetization curves between 0.1 and 1 T.

AFM transition. On the other hand, no peak is detected in the susceptibility for $x = 0.9$, although the susceptibility deviates from M/H below T_N. This is in contrast to the clear separation between the ZFC and FC data shown in Fig. 4. Although the origin of the absence of the χ peak is unclear at the moment, it seems to be consistent with the absence of the peak in the temperature dependence of the specific heat shown later. It should be pointed out that the AFM state for $x = 0.9$ corresponds to the AFM state for $x = 1$ above H_C because $NaCr_2O_4$ has a similar χ^{high}-T curve [17]. This is consistent with the expectation obtained from the x-H magnetic phase diagram.

All the samples show electrically insulating behavior as shown in Fig. 9. Arrhenius-type behavior is observed for $x = 0.1$ and 1 and the energy gap was estimated to be $\Delta = 1.65 \times 10^3$ K for $x = 0.1$, and 0.54×10^3 K for $T < T_N$ and 1.33×10^3 K for $T > T_N$ for $x = 1$. On the other hand, for $0.2 \leqslant x \leqslant 0.95$, ln ρ shows linearity against $1/T^{1/4}$, rather than against $1/T$, strongly suggesting variable-range hopping (VRH) in the compounds [34]. Thus, Anderson localization most likely takes place for $0.2 \leqslant x \leqslant 0.95$ due to the random potential caused by random distribution of Ca and Na ions.

VRH in $Ca_{1-x}Na_xCr_2O_4$ strongly suggests the compound would show metallic conductivity for $0.2 \leqslant x \leqslant 0.95$ in the absence of the random potential. This is quite reasonable because ligand holes tend to be itinerant as is expected from the Zaanen-Sawatzky-Allen (ZSA) phase diagram [35]. This diagram, however, can not explain the insulating nature of $NaCr_2O_4$. In general, as the oxidation state of the TM ions increases, the E_{CT} of the oxide becomes significantly smaller and the onsite Coulomb interaction becomes slightly larger. This is because the energy level of the $3d$ orbitals of the TM ions becomes lower and the $3d$ orbitals of the TM ions contract. In short, a position of the oxide on the ZSA phase diagram moves leftward and upward with increase in oxidation. The ZSA phase diagram has been modified to have an insulating region for $E_{CT} < 0$ [36], but there is no metallic region between the insulating regions for $E_{CT} < 0$ and for $E_{CT} > 0$; once an oxide becomes metallic by oxidation it will not become an insulator again by further oxidation. Therefore, even according to the modified ZSA phase diagram, $NaCr_2O_4$ should remain metallic because $Ca_{1-x}Na_xCr_2O_4$ would change from an insulator to a metal between $x = 0.1$ and 0.2 without the random potential. Because the $NaCr_2O_4$ is "reentrant" insulator, we look for possible reasons of insulating ground state that do not emerge from the modified ZSA phased diagram. One of the reasons is simply a change in the lattice parameters [16] that can destroy a metallic ground state. A more plausible explanation is due to a strong correlation effect, such as hole-phonon coupling or Coulomb interactions between the ligand holes. This explanation is supported by the fact that the insulating state with Arrhenius-type behavior appears when the Cr valence is exactly 3.5+. Slight deviation from this valence destroys the insulating state. It should be

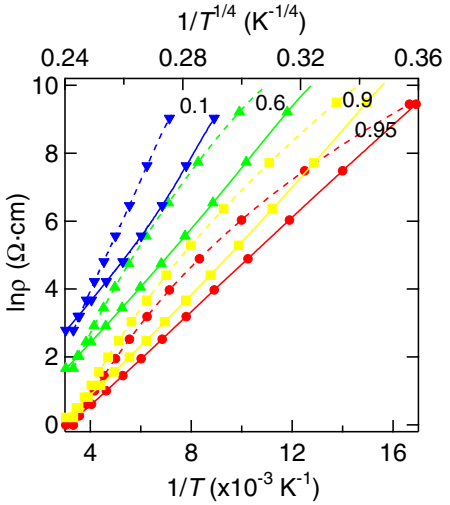

FIG. 9. (Color online) Electrical resistivity of $Ca_{1-x}Na_xCr_2O_4$ for $x = 0.1$ (blue downward triangles), 0.6 (green upward triangles), 0.9 (yellow squares), and 0.95 (red circles). The lines connect the observed data and the markers are placed every 50 data points. The broken and solid lines are for the bottom and top axes, respectively.

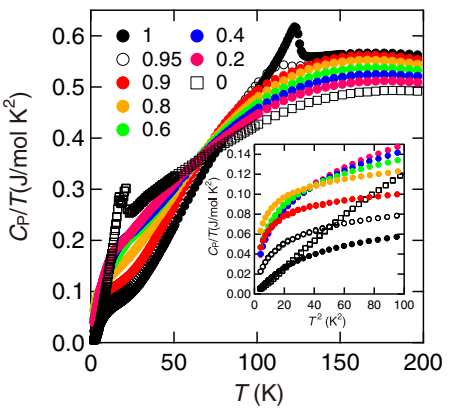

FIG. 10. (Color online) Specific heat of $Ca_{1-x}Na_xCr_2O_4$. The main panel and inset show T and T^2 dependencies of C_P/T, respectively. For monochromatic printouts, the C_P/T value at $T = 200$ K decreases from $x = 1$ to 0 while that at $T^2 = 100$ K^2 decreases from $x = 0.2$ to 1.

pointed out that the Peierls mechanism is proposed for the insulating state of $K_2Cr_8O_{16}$ [8].

Specific-heat data of $Ca_{1-x}Na_xCr_2O_4$ are shown in Fig. 10. Although $NaCr_2O_4$ shows a clear peak at T_N, the anomaly at T_N is obscure for $x = 0.95$ and eventually disappears for $x = 0.9$. This corresponds to the absence of the peak of magnetic susceptibility for $x = 0.9$. The double peaks in specific heat of β-$CaCr_2O_4$ agree with the previous report [15]. Although the C_P/T-T^2 curves are not linear even below 7 K for all the compounds except for β-$CaCr_2O_4$ (see inset in Fig. 10), the curves appear to reach finite values except for $NaCr_2O_4$ and β-$CaCr_2O_4$. This behavior seems reasonable because both the spin-glass state and Anderson localization cause finite specific heat at 0 K [37,38]. The C_P/T-T^2 curves appear to change qualitatively at around $x = 0.6$, below which the typical spin-glass behavior was observed. This implies that major origins of the finite values of 0-K specific heat change at $x \simeq 0.6$.

IV. CONCLUSIONS

Magnetic state of $Ca_{1-x}Na_xCr_2O_4$ changes drastically at around $x = 0.6$. The AFM transition appears above $x = \frac{2}{3}$ with decreasing T_N from $x = 1$ to $\frac{2}{3}$, while typical spin-glass behavior is found for $0.1 \leqslant x \leqslant 0.6$. Interestingly, the spin-glass behavior remains even for $\frac{2}{3} \leqslant x \leqslant 0.95$ coexisting with the AFM ordering. The AFM transition is clear in the temperature dependence of ZFC and FC magnetization, while it obscurely appears in the temperature dependencies of magnetic susceptibility and specific heat. The Curie constant is significantly smaller than the theoretical one, suggesting large quantum fluctuations due to spin frustrations and/or one-dimensional spin correlations. The difference between the observed and calculated values increases with increasing x, probably because of stronger hybridization between Cr and O ions for higher x values. Weiss temperature increases from $\Theta = -202$ K at $x = 0$ to 198 K at $x = 1$. This indicates that a ligand hole mediates FM interactions of approximately 400 K by double-exchange mechanism. The M_S^{low}, M_S^{high}, and χ^{low} at 2 K show an unusual peak at $x = 0.85$. Periodicity of magnetic ordering probably depends on x. Electrical resistivity for $x = 0.1$ and 1 obeys Arrhenius-type behavior with energy gaps of $\Delta = 1.65 \times 10^3$ K, and 0.54×10^3 for $T < T_N$ and 1.33×10^3 K for $T > T_N$, respectively. On the other hand, electrical resistivity for $0.2 \leqslant x \leqslant 0.95$ appears to be governed by variable-range hopping, and so Anderson localization likely takes place.

ACKNOWLEDGMENTS

The author thanks T. Taniguchi (NIMS) for his technical support for high-pressure synthesis, T. Kolodiazhnyi, M. Kohno, E. Takayama-Muromachi (NIMS), H. Takeda, M. Itoh (Nagoya University), J. Sugiyama, H. Nozaki (Toyota R&D Laboratory, Inc.), A. Irizawa (Osaka University), and J. Okamoto (KEK) for fruitful discussion. This study was supported in part by a Grant-in-Aid for Scientific Research (A) (Grant No. 22246083) and by "Funding Program for World-Leading Innovative R&D on Science and Technology (FIRST Program)" from the Japan Society for the Promotion of Science (JSPS).

[1] M. Takano, N. Nakanishi, Y. Takeda, S. Naka, and T. Takada, Mater. Res. Bull. **12**, 923 (1977).
[2] T. Takeda, R. Kanno, Y. Kawamoto, M. Takano, S. Kawasaki, T. Kamiyama, and F. Izumi, Solid State Sci. **2**, 673 (2000).
[3] J. B. Torrance, P. Lacorre, A. I. Nazzal, E. J. Ansaldo, and Ch. Niedermayer, Phys. Rev. B **45**, 8209 (1992).
[4] M. L. Medarde, J. Phys.: Condens. Matter **9**, 1679 (1997).
[5] M. A. Korotin, V. I. Anisimov, D. I. Khomskii, and G. A. Sawatzky, Phys. Rev. Lett. **80**, 4305 (1998).
[6] K. Hasegawa, M. Isobe, T. Yamauchi, H. Ueda, J. I. Yamaura, H. Gotou, T. Yagi, H. Sato, and Y. Ueda, Phys. Rev. Lett. **103**, 146403 (2009).
[7] P. Mahadevan, A. Kumar, D. Choudhury, and D. D. Sarma, Phys. Rev. Lett. **104**, 256401 (2010).
[8] T. Toriyama, A. Nakao, Y. Yamaki, H. Nakao, Y. Murakami, K. Hasegawa, M. Isobe, Y. Ueda, A. V. Ushakov, D. I. Khomskii, S. V. Streltsov, T. Konishi, and Y. Ohta, Phys. Rev. Lett. **107**, 266402 (2011).
[9] J. Sugiyama, H. Nozaki, M. Månsson, K. Prša, D. Andreica, A. Amato, M. Isobe, and Y. Ueda, Phys. Rev. B **85**, 214407 (2012).
[10] C. Zener, Phys. Rev. **82**, 403 (1951).
[11] P. W. Anderson and H. Hasegawa, Phys. Rev. **100**, 675 (1955).
[12] P.-G. de Gennes, Phys. Rev. **118**, 141 (1960).
[13] F. C. Zhang and T. M. Rice, Phys. Rev. B **37**, 3759 (1988).
[14] S. Nishimoto and Y. Ohta, Phys. Rev. Lett. **109**, 076401 (2012).
[15] F. Damay, C. Martin, V. Hardy, A. Maignan, G. André, K. Knight, S. R. Giblin, and L. C. Chapon, Phys. Rev. B **81**, 214405 (2010).
[16] H. Sakurai, T. Kolodiazhnyi, Y. Michiue, E. Takayama-Muromachi, Y. Tanabe, and H. Kikuchi, Angew. Chem. Int. Ed. **51**, 6653 (2012).
[17] H. Sakurai (unpublished).
[18] J. Okamoto *et al*. (unpublished).
[19] T. Kolodiazhnyi and H. Sakurai, J. Appl. Phys. **113**, 224109 (2013).
[20] T. Toriyama, A. Shimoi, T. Konishi, and Y. Ohta, Meeting abstract of the Physical Society of Japan **68**, 605 (2013) (in Japanese).
[21] B. Bleaney and K. W. H. Stevens, Rep. Prog. Phys. **16**, 108 (1953).
[22] K. D. Bowers and J. Owen, Rep. Prog. Phys. **18**, 304 (1955).
[23] J. W. Orton, Rep. Prog. Phys. **22**, 204 (1959), in which the g values of Cr^{3+} in $CrCl_3$ are listed to be $g = 2.00$ at 290 and 90 K, 2.09 at 20.4 K, and 2.37 at 13 and 15 K. The g values of more than 2 are probably due to antiferromagentic ordering at 16.8 K [39].
[24] J. E. Geusic, M. Peter, and E. O. Schulz-DuBois, Bell Syst. Tech. J. **28**, 291 (1959).
[25] P. T. Squire and J. W. Orton, Proc. Phys. Soc., London **88**, 649 (1966).

[26] A. V. Chichev, M. Dlouhá, S. Vratislav, K. Knížek, J. Hejtmánek, M. Maryško, M. Veverka, Z. Jirák, N. O. Golosova, D. P. Kozlenko, and B. N. Savenko, Phys. Rev. B **74**, 134414 (2006).
[27] M. Merz, D. Fuchs, A. Assmann, S. Uebe, H. v. Löhneysen, P. Nagel, and S. Schuppler, Phys. Rev. B **84**, 014436 (2011).
[28] J. J. Neumeier and D. H. Goodwin, J. Appl. Phys. **85**, 5591 (1999).
[29] H. Sakurai, Phys. Rev. B **78**, 094410 (2008).
[30] J. Sugiyama, Y. Ikedo, T. Goko, E. J. Ansaldo, J. H. Brewer, P. L. Russo, K. H. Chow, and H. Sakurai, Phys. Rev. B **78**, 224406 (2008).
[31] O. Ofer, Y. Ikedo, T. Goko, M. Mänsson, J. Sugiyama, E. J. Ansaldo, J. H. Brewer, K. H. Chow, and H. Sakurai, Phys. Rev. B **82**, 094410 (2010).
[32] H. Takeda, M. Itoh, and H. Sakurai, Phys. Rev. B **86**, 174405 (2012).
[33] H. Nozaki, M. Harada, H. Sakurai, E. Takayama-Muromachi, M. Mänsson, V. Pomjakushin, L. Keller, O. Ofer, E. J. Ansaldo, J. H. Brewer, and J. Sugiyama, Meeting abstract of the Physical Society of Japan **67**(1), 693 (2012) (in Japanese).
[34] N. F. Mott, *Metal-Insulator Transitions* (Taylor & Francis, London, 1974).
[35] J. Zaanen, G. A. Sawatzky, and J. W. Allen, Phys. Rev. Lett. **55**, 418 (1985).
[36] T. Mizokawa, A. Fujimori, H. Namatame, K. Akeyama, and N. Kosugi, Phys. Rev. B **49**, 7193 (1994).
[37] K. Binder and A. P. Young, Rev. Mod. Phys. **58**, 801 (1986).
[38] E. Yamaguchi, H. Aoki, and H. Kamimura, J. Phys. C: Solid State Phys. **12**, 4801 (1979).
[39] R. W. Bené, Phys. Rev. **178**, 497 (1969).